Supporting Information

The length of the calmodulin linker determines the extent of transient interdomain association and target affinity

Nicholas J. Anthis and G. Marius Clore*

Laboratories of Chemical Physics, National Institute of Diabetes and Digestive and Kidney Diseases, National Institutes of Health, Bethesda, Maryland 20892-0520, USA

Experimental Procedures

Protein production, paramagnetic tagging, mutagenesis, and sample preparation

The full-length 148-residue human calmodulin (CaM) protein, and its N- (residues 1-76) and C- (residues 81-148) terminal domains were expressed and purified as described previously for full-length CaM.[S1] Proteins were either uniformly $^{2}H/^{13}C/^{15}N$-labeled or at natural isotopic abundance. After purification, CaM was exchanged into the "NMR buffer", which consisted of 5% D_2O/95% H_2O, 8 mM $CaCl_2$, 100 mM KCl, 1× Roche cOmplete Protease Inhibitor, 0.02% sodium azide, and 25 mM HEPES, pH 6.5. Samples were concentrated to 0.3 mM with Amicon Ultra Centrifugal Filter Units (3 kDa molecular weight cutoff). All NMR experiments were conducted in "NMR buffer". Fluorescence experiments were conducted in the "fluorescence buffer", which consisted of 100% H_2O, 3 mM $CaCl_2$, and 10 mM MES, pH 5.5. For fluorescence experiments, concentrated stocks of CaM in NMR buffer were diluted into the "fluorescence buffer". Concentrations were determined by absorbance at 280 nm (for CaM 1-148 and 81-148, ε_{280} = 2,980), except for CaM 1-76, which contains no groups that absorb at 280 nm. For the latter construct, concentrations mere measured by absorbance at 205 nm, using a molar absorptivity (extinction coefficient) of ε_{205} = 266,150 $M^{-1}\cdot cm^{-1}$, which was calculated from the amino acid sequence as previously described, using the server at http://spin.niddk.nih.gov/clore.[S2]

All mutations (including those in the CaM linker and the A128C mutation in the C-terminal domain for spin labeling) were made using the QuikChange Site-Directed Mutagenesis Kit (Agilent). CaM A128C was paramagnetically labeled by the addition of a 10-fold excess of the nitroxide spin-label (1-Oxyl-2,2,5,5-tetramethyl-δ-3-pyrroline-3-methyl) methanethiosulfonate ("MTSL"; Toronto Research Chemicals) to ~200 μM CaM. The reaction was allowed to proceed in the dark for 2 hours and tested for completion by mass spectrometry. The diamagnetic control was labeled by the same method using (1-Acetoxy-2,2,5,5-tetramethyl-δ-3-pyrroline-3-methyl) methanethiosulfonate (Toronto Research Chemicals). Unreacted spin-label was removed with a HiPrep 26/10 Desalting Column (GE Life Sciences) as CaM was exchanged into "NMR buffer".

For NMR experiments on peptide-bound CaM (CaM-4Ca^{2+}-MLCK), CaM was mixed with 1.2 equivalents of target peptide (skeletal muscle myosin light chain kinase, skMLCK, M13 peptide; commercially synthesized by Anaspec; KRRWKKNFIAVSAANRFKKISSSGAL). Fluorescence experiments were conducted on an M13 peptide with a 5-carboxy-X-rhodamine (5ROX) label conjugated to its N-terminus (custom-synthesized by Anaspec).

NMR spectroscopy

NMR experiments were performed on uniformly $^{2}H/^{13}C/^{15}N$-labeled CaM-4Ca^{2+}, including wild-type (WT) and mutant constructs. Data were recorded at 27°C on a Bruker 600 MHz spectrometer equipped with a triple resonance *z*-gradient cryoprobe. Data were processed using

NMRPipe[S3] and analyzed with the programs XIPP (in-house software written by D.S. Garrett) or Sparky (www.cgl.ucsf.edu/home/sparky).

Transverse $^{1}H_N$-Γ_2 PRE rates were obtained from the differences in the transverse $^{1}H_N$-R_2 relaxation rates between the paramagnetic and diamagnetic samples[S4] using a 2D TROSY pulse scheme with a variable delay performed at the end of the pulse sequence, thus measuring the TROSY component of $^{1}H_N$-R_2.[S1] Two time points (separated by 20 ms) were used for the $^{1}H_N$-R_2 measurements, and the errors in the $^{1}H_N$-Γ_2 PRE rates were calculated from spectral noise as described previously.[S5] Samples for PRE experiments contained 0.3 mM $^{2}H/^{13}C/^{15}N$-labeled CaM-4Ca^{2+}, tagged with a spin labeled or diamagnetic control tag at A128C. Experiments were also performed to measure intermolecular PREs; these measurements were made on 0.3 mM $^{2}H/^{13}C/^{15}N$-labeled CaM (1-76 or 1-148) with no attached spin label in the presence of 0.3 mM CaM (81-148 or 1-148, respectively) at natural isotopic abundance, spin-labeled at A128C. In this manuscript, the PREs for a given molecule are reported as the ratio of the PREs for that molecule to those of the WT. This ratio was determined by plotting the PREs of the molecule in question on the *y*-axis, plotting the PREs of the WT on the *x*-axis, and taking the slope of a best-fit straight line through the data.

^{15}N T_1 and $T_{1\rho}$ were measured with a TROSY readout using the pulse sequences described by Lakomek et al.[S6] on 0.3 mM $^{2}H/^{13}C/^{15}N$-labeled CaM-4Ca^{2+} (tagged at A128C with the diamagnetic control label, unless otherwise stated). Experiments were performed with 8 time points spanning from 0 to ~1.3 times T_1 or $T_{1\rho}$. T_1 and $T_{1\rho}$ values were calculated for each residue by fitting peak intensities to a single exponential decay. T_2 values were calculated from T_1 and $T_{1\rho}$ using the equation:

$$T_2 = \sin^2\theta / [(1/T_{1\rho}) - (1/T_1)\cos^2\theta] \qquad \text{(S1)}$$

where the angle θ is given by:

$$\theta = \tan^{-1}(\omega_1 / \delta\omega) \qquad \text{(S2)}$$

where ω_1 is the strength of the spin-lock field (1 kHz in this study) and $\delta\omega$ is the difference in frequency (in the ^{15}N dimension, in Hz) between the peak and the transmitter frequency. Overall rotational correlation times (τ_c) were estimated using the equation:

$$\tau_C = (1/2\omega_N)\sqrt{(6T_1/T_2 - 7)} \qquad \text{(S3)}$$

where τ_c is in units of seconds and ω_N is the ^{15}N frequency in radians·s^{-1}. The value of T_1/T_2 reported for each domain in Table S1 is the average for residues that are not in flexible loops or linkers and that do not exhibit T_1 or T_2 values outside of 1 standard deviation of the average for each domain. The value of τ_c for each domain was determined by optimizing a single value of τ_c that best fits all selected T_1/T_2 ratios within a given domain using Eq. S3. The uncertainties in the optimized values of τ_c are given in Table S1.

Fitting CaM linker data to a random coil model

To advance our understanding of the role of the CaM linker, a theoretical framework was applied to the analysis of the interdomain PRE data, interpreting this data through values of effective molarity (M_{eff}) and effective concentration ($conc_{eff}$). Specifically, we applied a framework based on a random coil model described by Krishnamurthy et al.[S7] To accomplish this, we converted the experimental interdomain PRE data for each linker mutant into values of M_{eff}. For each mutant, we took the ratio of the measured interdomain PREs of the mutant to those of WT CaM (i.e. the slope of the red lines in Figure 2); in this study, the term "PREs" generally refers to this ratio as opposed to the raw PRE data. We describe linker length using the variable Δn, which corresponds to the number of residues added (positive) or removed (negative) from the

WT linker (Δn = 0 for the WT linker). M_{eff} relates the strength of the intramolecular interaction for a given linker to that of the intermolecular interaction and is defined by the ratio of equilibrium constants:[S7]

$$M_{\text{eff}} = K_{\text{D}}^{\text{intermol}} / K_{\text{D}}^{\text{intramol}} \tag{S4}$$

$K_{\text{D}}^{\text{intermol}}$ is the bimolecular equilibrium constant for the intermolecular interaction, given in concentration units:

$$K_{\text{D}}^{\text{intermol}} = \frac{[\text{CaM}_{\text{N}}]_{\text{free}}[\text{CaM}_{\text{C}}]_{\text{free}}}{[\text{CaM}_{\text{N}}\text{CaM}_{\text{C}}]_{\text{associated}}} \tag{S5}$$

$K_{\text{D}}^{\text{intramol}}$ is the unimolecular equilibrium constant for the intramolecular interaction, which is dimensionless:

$$K_{\text{D}}^{\text{intramol}} = \frac{[\text{CaM}]_{\text{extended}}}{[\text{CaM}]_{\text{associated}}} \tag{S6}$$

Here, we consider three different populations of CaM-4Ca^{2+} in the absence of peptide (Figure S3). Population 1, the major population, comprises the conformations where the two domains are tumbling essentially independently of one another (and bound only by the linker, if present). Population 2 is a minor state that comprises the two linked domains interacting with one another. For the WT linker, we previously demonstrated that population 2 comprises 5-10% of the total population.[S1] The PREs from population 2 (interdomain, intramolecular) are denoted as $\Gamma_2^{\text{intramol}}$. Population 3 represents an even smaller population (~1-2%) of domains interacting intermolecularly. The PREs from Population 3 (interdomain, intermolecular) are denoted as $\Gamma_2^{\text{intermol}}$. Because the interdomain PREs in CaM display a similar profile to the intermolecular PREs (Figure 2), [S1] we can make the assumption that they are both due to the same type of interaction between an N- and C-terminal domain. Because these processes take place on a timescale that is fast on the PRE time scale, the total PRE (Γ_2^{tot}) for a given nucleus in the N-terminal domain when the C-terminal domain is tagged with a paramagnetic group is the sum of the intramolecular interdomain PREs and the intermolecular PREs:

$$\Gamma_2^{\text{tot}} = \Gamma_2^{\text{intramol}} + \Gamma_2^{\text{intermol}} \tag{S7}$$

Γ_2^{tot} and $\Gamma_2^{\text{intramol}}$ are functions of Δn. The value of $\Gamma_2^{\text{intermol}}$, which is derived in this study from the interdomain PREs measured between isolated domains, is constant and does not depend on Δn. This trend will be the same for other variables and constants in this study; all "intramol" and "tot" variables are dependent on Δn, whereas "intermol" will always signify a constant that is not affected by Δn. Γ_2^{tot} and $\Gamma_2^{\text{intermol}}$ are both dependent on the concentration of the spin-labeled domain (M_{ind}), which in this study is kept constant at 0.3 mM to simplify analysis and make all results directly comparable. $\Gamma_2^{\text{intramol}}$, on the other hand, is independent of protein concentration. We make the assumption that the populations of the transiently associated states are small enough that they do not directly compete with one another. Thus, for a given linker, the ratio of the intramolecular PREs to the universal intermolecular PREs is equal to the ratio of M_{eff} to M_{ind}:

$$\frac{\Gamma_2^{\text{intramol}}}{\Gamma_2^{\text{intermol}}} = \frac{M_{\text{eff}}}{M_{\text{ind}}} \tag{S8}$$

Combining Eq. S7 and S8, we can calculate M_{eff} for any CaM linker mutant as:

$$M_{\text{eff}} = M_{\text{ind}}\left(\Gamma_2^{\text{tot}}/\Gamma_2^{\text{ind}} - 1\right) \tag{S9}$$

Eq. S9 is presented in the main text as Eq. 1. These empirical values of M_{eff} can then be compared to theoretical values of effective concentration, $conc_{eff}$, calculated using a random coil model for the CaM linker (Figure S4); $conc_{eff}$ is a theoretical term related to the probability of the two ends of a molecule coming together.[S7] In this study, M_{eff} and $conc_{eff}$ are treated as functionally equivalent, with the distinction being that M_{eff} is an empirical observation and $conc_{eff}$ is a theoretical value calculated from a random coil model. Here we use a random coil model described by Krishnamurthy et al.[S7] for the $conc_{eff}$ of two points at opposite ends of random-coil linker that only interact when located at a defined distance d from each other. An illustration of this model is shown in Figure S4A. The alternative representation in Figure S4B shows how this model qualitatively relates to CaM. As this model here is intended to be a simplistic representation of CaM and its flexible linker, the values of the fitted parameters should be taken at face value. Using this model, $conc_{eff}$ is given by the following equation, which is also presented as Eq. 2 in the main text:

$$conc_{\mathrm{eff}} = \left(\frac{3}{2\pi}\right)^{3/2} \frac{p}{N_{\mathrm{A}}\left(< r^2 >^{1/2}\right)^3} \exp\left(\frac{-3d^2}{2\left(< r^2 >^{1/2}\right)^2}\right) \qquad \text{(S10)}$$

where N_A is Avogadro's number (6.0221×10^{23} mol^{-1}), and p is a dimensionless constant that takes into account both the excluded volume occupied by the protein domain and the orientational requirement of the interdomain interaction. The root-mean-square distance (rmsd) between ends of the random coil is given by:

$$< r^2 >^{1/2} = l\sqrt{C(n_0 + \Delta n)} \qquad \text{(S11)}$$

where l is the length of each unit of the chain (here fixed at 3.8 Å for the average length of the backbone of one amino acid residue). The number of units in the WT linker is given by n_0 (i.e. the linker of a given molecule contains $n = n_0 + \Delta n$ units). The constant C is the characteristic ratio of a random-coil polymer:

$$C = < r^2 > / nl^2 \qquad \text{(S12)}$$

C is described in detail by Cantor and Schimmel.[S8] In brief, C is a measure of the stiffness of the polymer, and $C = 1$ for a totally unconstrained random-coil polymer. In a biological polymer, however, C is greater than 1 and is dependent on n for small values of n, reaching an n-independent limit of C_∞ at large values of n. A polyglycine chain reaches C_∞ = 1.9-2.1 at $n \sim 6$. A polyalanine chain, however, exhibits a larger value of C for all values of n, but only approaches C_∞ = 9.0 near $n \sim 80$. For our purposes here, we used a fixed value of $C = 2$, roughly corresponding to the value expected for a polyglycine chain. (For example, a value of $C = 1.9$ is expected for a polyglycine chain of 5 units; even for a much stiffer polyalanine chain of 5 residues, C is only increased to 3.4.) Thus, $C = 2$ was deemed an appropriate value for this system.

The pre-exponential portion of Eq. S10 describes the inverse cube relationship between $conc_{eff}$ and the rmsd between the two ends of the linker. This is strictly based on the three-dimensional space sampled by the two ends of the linker, and it predicts a decreasing $conc_{eff}$ as the linker is lengthened. Depending on the desired units of concentration and the units of length used, a conversion factor may need to be included. The exponential portion of Eq. S10, on the other hand, describes the requirement of the interaction on the two ends of the linker being a specific distance d apart. Note that this distance d is not the distance between the surfaces of the two domains or the centers of mass of the two domains, but the distance between the ends of the linker when the two domains are in contact.

Eq. S11 was fit to the empirical data (M_{eff} vs. Δn), keeping l and C constant, and optimizing the values of d, p, and n_0 (Figure 3; fit in red, pre-exponential portion in green, exponential portion in blue). The fit was performed by minimizing the difference between the calculated $conc_{eff}$ values and the empirical M_{eff} values for each value of Δn. This fit was performed in MATLAB, and errors of the fitted parameters were estimated using Monte Carlo analysis, assuming an error in M_{eff} of 10%.

Fluorescence experiments

Fluorescence experiments were carried out at 37°C using a Jobin Ybon FluoroMax-3 fluorometer equipped with a Peltier temperature control unit. A 1 cm × 1 cm quartz cuvette was used (Starna Cells, Inc.). The fluorescence anisotropy of 5ROX-MLCK was monitored with excitation at 583 nm and emission at 607 nm. Measurements were acquired on 1 nM 5ROX-MLCK in the presence of 0-1 nM CaM 1-148 or 0-1.3 μM CaM 1-76 + CaM 81-148 (for the separated domains, a stock containing an equal concentration of the two domains was made and titrated into the fluorescent peptide).

Data were analyzed by fitting the fluorescence anisotropy versus CaM concentration to the following equation:

$$A = A_{min} + A_{max}\left(\frac{[F]_{tot} + [U]_{tot} + K_D - \sqrt{([F]_{tot} + [U]_{tot} + K_D)^2 - 4[F]_{tot}[U]_{tot}}}{2[F]_{tot}}\right) \quad \text{(S13)}$$

where A is the measured fluorescence anisotropy at each point (the dependent variable in the fitting); A_{max} the anisotropy of the MLCK peptide fully saturated with CaM; A_{min} the anisotropy of the free 5ROX-MLCK peptide; $[F]_{tot}$ the total (bound + unbound) concentration of the MLCK peptide ("F" for "fluorescent"); $[U]_{tot}$ the total (bound + unbound) concentration of CaM at each point (the independent variable in the fitting; "U" for "unseen"); and K_D the equilibrium dissociation constant, defined as:

$$K_D = \frac{[U][F]}{[UF]} \quad \text{(S14)}$$

Although this is the true K_D in most cases, for the titration of the MLCK peptide with the two separated domains this is an apparent K_D describing the concentration at half saturation. Data were fit using OriginPro 8.

The conditions used for the fluorescence experiments (low salt, low pH, high temperature) were chosen to weaken the CaM/target interaction to assist in accurate affinity measurement. Under the conditions used for NMR, the K_D of WT CaM-4Ca^{2+} for 5ROX-M13 is ~ 10-30 pM (Table S1), but it was difficult to determine an accurate value within the sensitivity limits of the experiment. The temperature was increased from 27ºC to 37ºC, which, due to the fact that the interaction is highly exothermic,[S1] was expected to decrease the affinity by a factor of ~2. In addition, based on results found in the literature on similar peptides,[S9,10] we predicted that lowering the pH from 6.5 to 5.5 and decreasing the ionic strength from [KCl] = 200 mM to 100 mM would decrease the affinity by approximately 10 to 100 fold. The ~20-to-40-fold reduction in affinity (to K_D ~ 400 pM) observed under these conditions was thus within the expected range. Despite the achieved decrease in affinity, low concentrations of CaM and 5ROX-M13 were still required. To prevent protein or peptide adsorption in the dilute samples, all dilutions were performed in Eppendorf Protein LoBind Tubes.

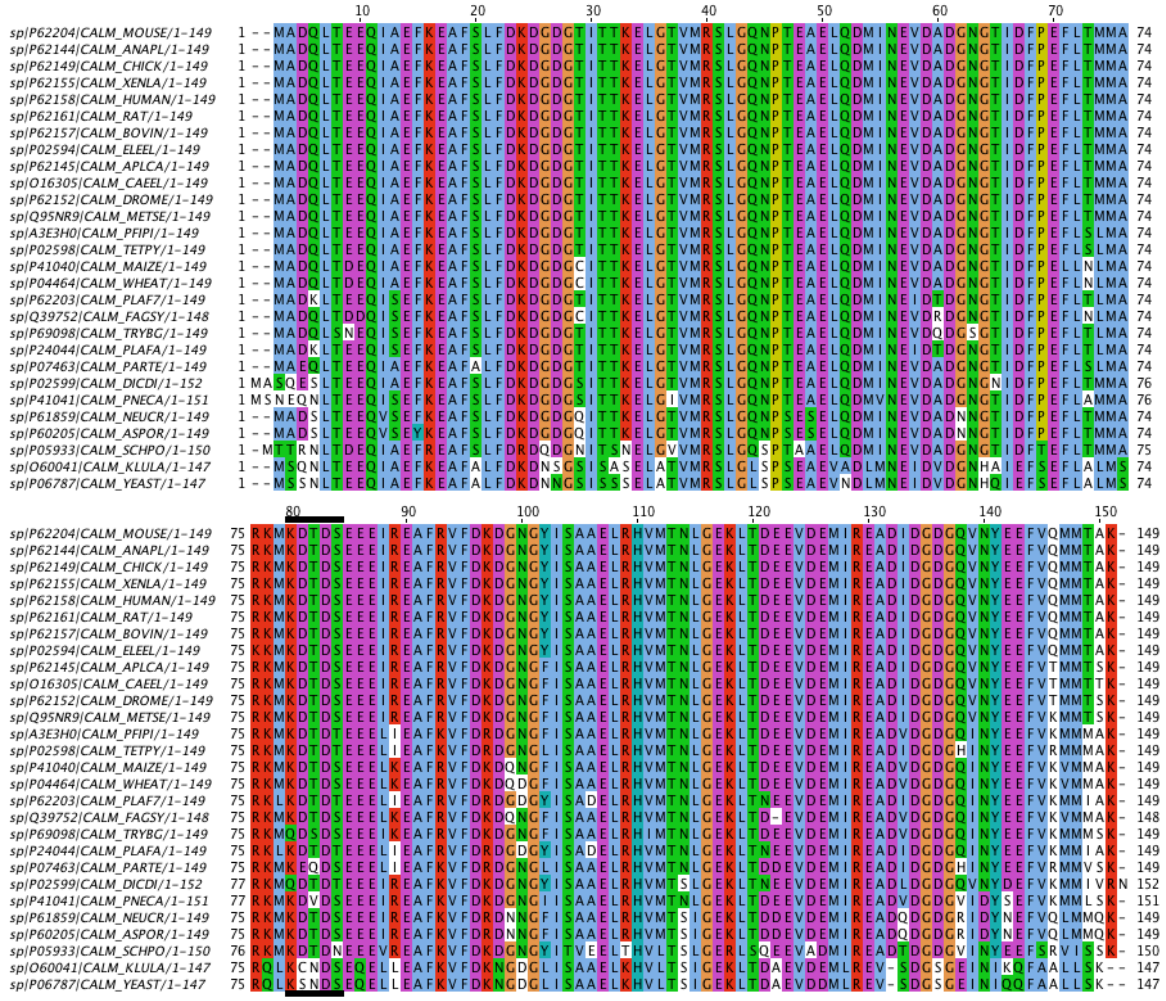

Figure S1. Alignment of a selection of calmodulin (CaM) sequences. Amino acid sequences of CaM from an assortment of organisms were aligned using the Clustal Omega[S11] web server on the EMBL-EBI website.[S12] Sequences were sorted and displayed in Jalview.[S13] Vertebrate sequences are located at the top and yeast sequences at the bottom. Others are found in between. Sequences are colored by amino acid type and identity. The UniProt[S14] accession number and entry name is given for each. The full UniProt entry is displayed for each, including the N-terminal methionine, which does not appear in the final processed protein sequence; thus, the numbering differs from that used in the rest of this study (and the numbers at the top correspond to the numbering of the longest sequence). The five-residue flexible linker is indicated by a black bar (beginning with number 80, but corresponding to residues 77-81 in the final processed human sequence). Note that the sequence of CaM is highly conserved, including that of the linker.

Figure S2. Mutations in the CaM linker used in this study. (A) Deletion and insertion mutations used to change the length of the CaM linker. (B) Other mutations used to alter the sequence and/or properties of the CaM linker. Additionally, the C-terminus of the N-terminal domain construct and the N-terminus of the C-terminal domain construct are shown. In both panels, CaM residues 70-90 are shown, and residues 77-81 (the flexible linker) are highlighted in red.

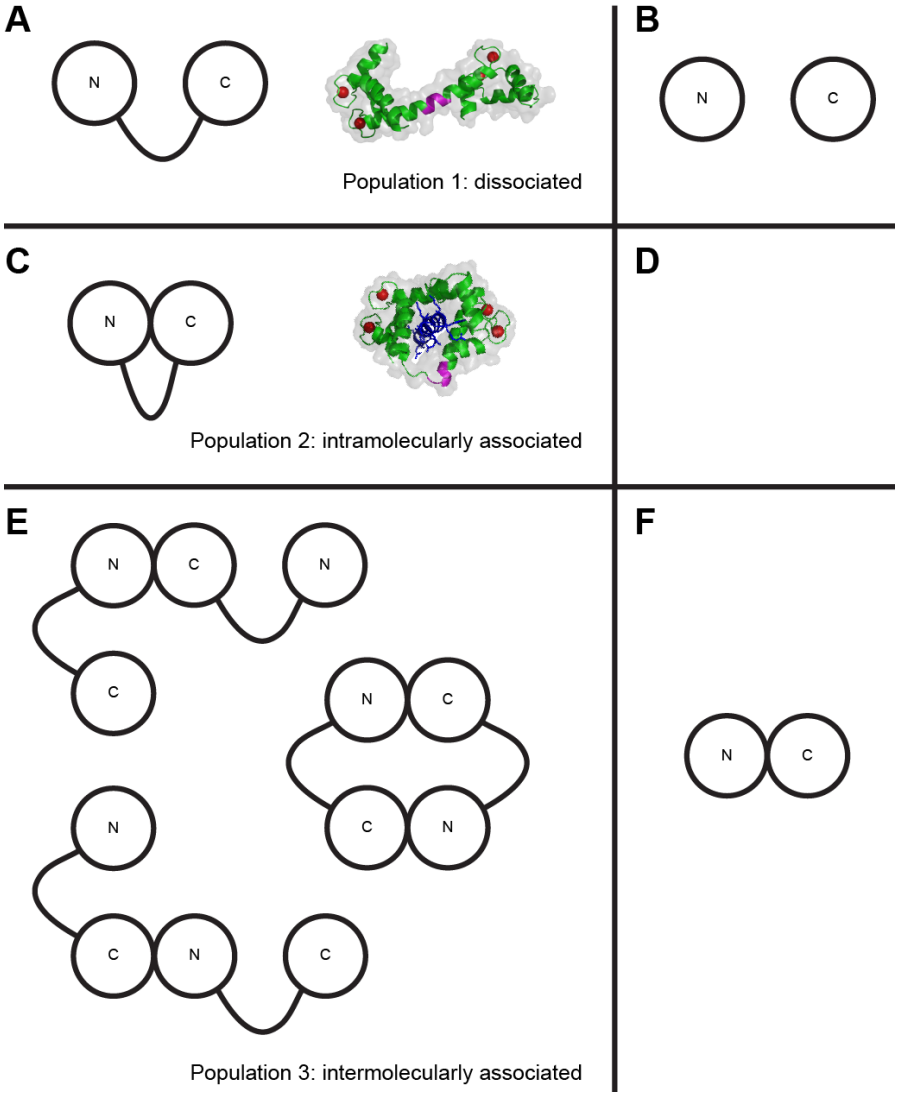

Figure S3. Summary of the different populations of CaM-4Ca^{2+}. CaM-4Ca^{2+} exists as an ensemble of states in equilibrium between three different populations. The panels on the left (A, C, E) show the populations for two CaM domains connected by a flexible linker (i.e. the natural state of CaM), and the panels on the right (B, D, F) show the populations for the isolated domains of CaM when the linker has been removed (i.e. an artificial situation). In population 1 (A, B), which is the major state, the two domains are dissociated from one another. In population 2 (C, D) and 3 (E, F), the N- and C-terminal domains are associated with each other. These are sparsely populated minor states (~5-10% for population 2; ~1-2% for population 3). Panel D is empty because intramolecular association is not possible for isolated domains. Although Panels C, E, and F, show different types of association between domains, it is assumed in this study that the interface between the N- and C-terminal domains is the same in each case, based on our previous results[S1] and the high correlation between intra- and intermolecular PREs (Figure 2), although panel E indicates that the intermolecular complex could take various forms. The extended dumbbell structure of CaM-4Ca^{2+} (PDB 1CLL)[S15] is shown in panel A, as a representation of one of the conformations that might be sampled in population 1. The compact structure of CaM-4Ca^{2+}-MLCK (PDB 1CDL)[S16] is shown in panel C, as an approximation of the interdomain conformation in population 2. The flexible linker is highlighted in magenta.

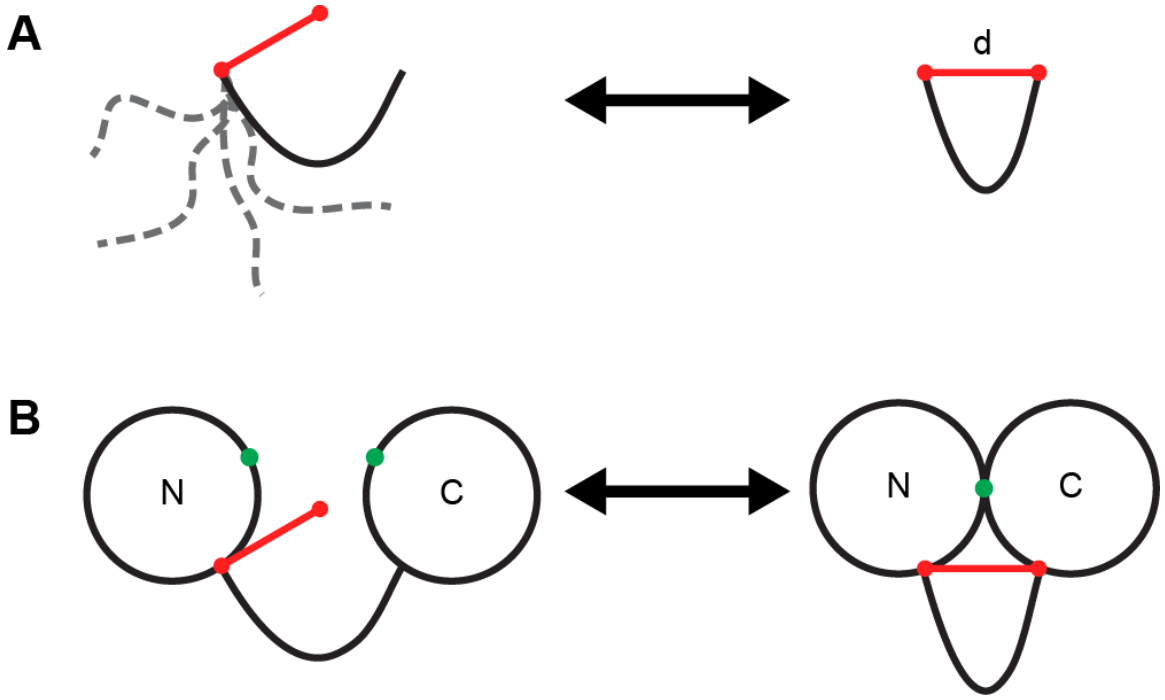

Figure S4. Illustration of the random-coil model used to model the CaM linker. (A) A random-coil chain (black) forms an interaction only when its two ends are located a certain distance (*d*, red) apart. The dotted grey lines represent the flexibility of the random-coil chain (left), which becomes restrained when forming its interaction (right). This model is the basis of Eq. 2 and Eq. S10, as described by Krishnamurthy et al.[S7] (B) A more realistic representation of CaM-4Ca^{2+} with its domains in the dissociated (left) and associated (right) states. The interaction surface is denoted by a green circle. The qualitative similarities between panels A and B support the use of the simple random-coil model to explain the behavior of the CaM linker.

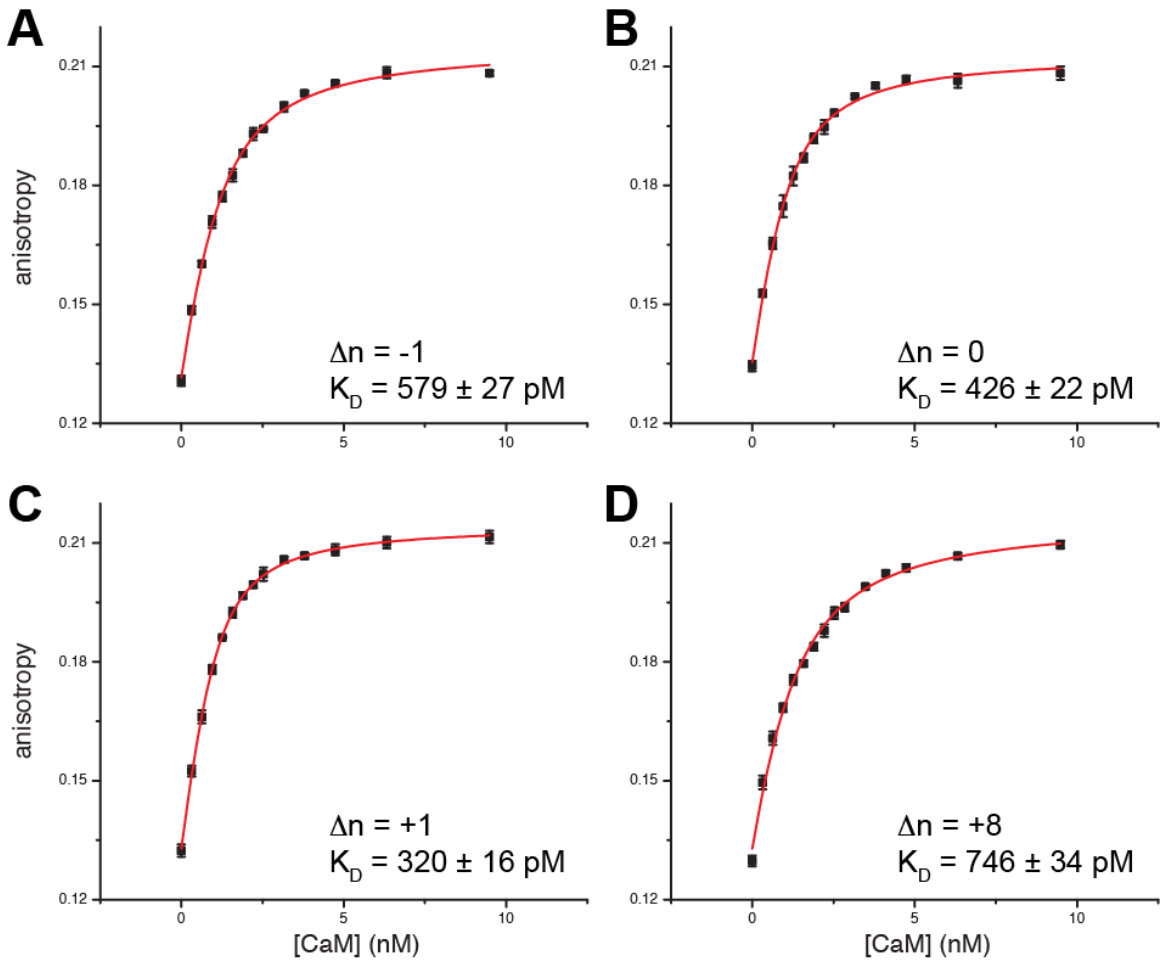

Figure S5. Sample fluorescence anisotropy titration curves. Fluorescence anisotropy was measured for 5ROX-M13 alone (1 nM) and in the presence of 0-10 nM CaM-4Ca^{2+}. Experimental data (average of three measurements) are plotted as filled-in squares, with error bars indicating one standard deviation. The best-fit line is shown in red. The linker length mutation (Δn) and K_D are indicated. Data are shown for linkers with Δn values of (A) -1, (B) 0, (C) +1, and (D) +8.

Table S1. Summary of experimental data

linker, condition[a]	^1H_N PRE		M_{eff} (mM)[d]	^{15}N relaxation								K_D (pM)[i]	
				T_1/T_2[e]				τ_c[h]					
	intradom[b]	interdom.[c]		free[f]		bound[g]		free		bound		low affinity[j]	high affinity[k]
				N-term	C-term	N-term	C-term	N-term	C-term	N-term	C-term		
-1	1.11	0.78	0.78	8.43 ± 1.04	7.71 ± 1.30			8.62 ± 0.05	8.17 ± 0.06			579 ± 27	
WT[l]	1[q]	1[q]	1.09	7.19 ± 0.68	6.72 ± 0.87	9.60 ± 0.64	9.95 ± 0.77	7.86 ± 0.04	7.53 ± 0.07	9.29 ± 0.07	9.49 ± 0.06	426 ± 22	13.6 ± 3.6
+1	0.98	1.28	1.47	7.00 ± 0.57	6.38 ± 0.52			7.73 ± 0.04	7.31 ± 0.07			320 ± 16	
+2	0.94	1.07	1.18										
+3	0.89	1.16	1.30										
+4	0.88	1.14	1.28	6.16 ± 0.55	5.70 ± 0.67			7.15 ± 0.05	6.81 ± 0.08				
+6	0.88	0.98	1.06										
+8	0.77	0.74	0.72	5.82 ± 0.45	5.32 ± 0.54	9.76 ± 0.86	10.11 ± 0.77	6.91 ± 0.05	6.52 ± 0.08	9.38 ± 0.09	9.57 ± 0.06	746 ± 34	
AAAAA	1.40	0.57	0.49	10.30 ± 0.86	9.72 ± 1.44			9.67 ± 0.07	9.34 ± 0.06			780 ± 37	
GGGGG	0.94	1.10	1.23	6.75 ± 0.59	6.17 ± 0.61			7.56 ± 0.05	7.15 ± 0.07			387 ± 19	
N-term[m]	[r]	0.22	0[q]	3.15 ± 0.23				4.51 ± 0.03				217,000 ± 11,000	
C-term[n]	0.46				2.66 ± 0.17				3.91 ± 0.13				
WT, intermol.[o]	1[q]	0.16	-0.08[s]										
WT, no tag[p]				7.32 ± 0.74	6.84 ± 0.91	9.17 ± 0.63	9.44 ± 0.52	7.94 ± 0.05	7.61 ± 0.07	9.06 ± 0.05	9.21 ± 0.06		23.6 ± 5.4[t]

[a]Data were measured and analyzed as described in Experimental Procedures. PREs were measured with CaM-4Ca^{2+} tagged with MTSL at position A128C in the C-terminal domain. Values of ^{15}N T_1 and T_2, unless otherwise stated, were measured on CaM-4Ca^{2+} conjugated to a diamagnetic control tag at A128C. Values of K_D, unless otherwise stated, were measured on CaM-4Ca^{2+} conjugated to MTSL at A128C.
[b]Ratio of the intradomain PREs (measured in the C-terminal domain for CaM paramagnetically tagged in the C-terminal domain) for CaM with the indicated linker relative to that of CaM with a WT linker.
[c]Ratio of the interdomain PREs (measured in the N-terminal domain for CaM paramagnetically tagged in the C-terminal domain) for CaM with the indicated linker relative to that of CaM with a WT linker.
[d]Calculated from interdomain PRE data as described in Experimental Procedures.
[e]Ratio of backbone ^{15}N T_1 to ^{15}N T_2, given as the average ± 1 s.d. for structured residues within either the N- or C-terminal domain.
[f]CaM-4Ca^{2+} in the absence of peptide.
[g]CaM-4Ca^{2+} bound to the MLCK peptide.
[h]Overall rotational correlation time calculated from T_1/T_2, as described in Experimental Procedures, given as the best-fit value ± 1 s.d..
[i]Affinity of CaM-4Ca^{2+} for 5ROX-MLCK, measured by fluorescence anisotropy, given as the best-fit value ± 1 s.d..
[j]Affinity measured under lower affinity conditions: higher temperature and "fluorescence buffer" (lower salt, lower pH).
[k]Affinity measured under higher affinity conditions: lower temperature and "NMR buffer" (higher salt, higher pH).

Footnotes to Table S1 (cont.)

[l]Here, WT (wild type) refers only to the CaM linker ($\Delta n = 0$), because this CaM sample has an A128C mutation, where MTSL or a diamagnetic control tag is conjugated.

[m]CaM 1-76. Values of M_{eff} and K_D were determined in concert with the C-terminal domain of CaM.

[n]CaM 81-148. Values of M_{eff} and K_D were determined in concert with the N-terminal domain of CaM.

[o]For this sample, PREs were measured on $^{2}H/^{13}C/^{15}N$ CaM-4Ca^{2+} in the presence of natural-abundance (NMR-invisible) CaM-4Ca^{2+} A128C-MTSL.

[p]For this sample, ^{15}N relaxation and affinity measurements were made on CaM-4Ca^{2+} with the full wild-type (WT) sequence (A128C, no tag).

[q]Equal to 0 or 1 by definition.

[r]Blank cells indicate measurements that are either not applicable or were not determined.

[s]This negative value is a result of the interdomain PRE ratio being slightly smaller for the intermolecular PRE measurements on full-length CaM, compared with those measured on the individual domains.

[t]Compare to $K_D = 50 \pm 50$ pM, determined by less-sensitive tryptophan fluorescence in our previous study.[S17]

Table S2. Error analysis for PRE correlation plots

linker	intradomain[a]				interdomain[b]			
	m			*R*	*m*			*R*
-1	1.11	±	0.047	0.99	0.78	±	0.023	0.98
+1	0.98	±	0.041	0.99	1.28	±	0.033	0.98
+2	0.94	±	0.053	0.98	1.07	±	0.033	0.98
+3	0.89	±	0.046	0.98	1.16	±	0.038	0.97
+4	0.88	±	0.038	0.99	1.14	±	0.032	0.98
+6	0.88	±	0.038	0.99	0.98	±	0.032	0.97
+8	0.77	±	0.054	0.97	0.74	±	0.029	0.96
AAAAA	1.40	±	0.077	0.98	0.57	±	0.027	0.95
GGGGG	0.94	±	0.038	0.99	1.10	±	0.043	0.97
N-term					0.22	±	0.028	0.72
C-term	0.46	±	0.057	0.92				

[a]The intradomain PREs (measured in the C-terminal domain for CaM paramagnetically tagged in the C-terminal domain) for CaM with the indicated linker were plotted on the *y*-axis, and those of CaM with a WT linker were plotted on the *x*-axis. The data were fit to a straight line through the origin, and the slope (*m*; ± 1 s.d.) and the correlation coefficient (*R*) are reported here.
[b]The same procedure as in footnote *a* was performed for interdomain PREs (measured in the N-terminal domain for CaM paramagnetically tagged in the C-terminal domain).

Supporting References

(S1) Anthis, N. J.; Doucleff, M.; Clore, G. M. *J. Am. Chem. Soc.* **2011**, *133*, 18966-18974.
(S2) Anthis, N. J.; Clore, G. M. *Protein Sci* **201**, *22*, 851-858.
(S3) Delaglio, F.; Grzesiek, S.; Vuister, G. W.; Zhu, G.; Pfeifer, J.; Bax, A. *J. Biomol. NMR* **1995**, *6*, 277-293.
(S4) Clore, G. M.; Iwahara, J. *Chem. Rev.* **2009**, *109*, 4108-4139.
(S5) Iwahara, J.; Tang, C.; Clore, G. M. *J.Magn. Reson.* **2007**, *184*, 185-195.
(S6) Lakomek, N. A.; Ying, J.; Bax, A. *J. Biomol. NMR* **2012**, *53*, 209-221.
(S7) Krishnamurthy, V. M.; Semetey, V.; Bracher, P. J.; Shen, N.; Whitesides, G. M. *J. Am. Chem. Soc.* **2007**, *129*, 1312-1320.
(S8) Cantor, C. R.; Paul, R. S. *Biophysical Chemistry: Part III: The Behavior of Biological Macromolecules*; W. H. Freeman, San Francisco, 1980.
(S9) Andre, I.; Kesvatera, T.; Jonsson, B.; Linse, S. *Biophys. J.* **2006**, *90*, 2903-2910.
(S10) Andre, I.; Kesvatera, T.; Jonsson, B.; Akerfeldt, K. S.; Linse, S. *Biophys. J.* **2004**, *87*, 1929-1938.
(S11) Sievers, F.; Wilm, A.; Dineen, D.; Gibson, T. J.; Karplus, K.; Li, W.; Lopez, R.; McWilliam, H.; Remmert, M.; Soding, J.; Thompson, J. D.; Higgins, D. G. *Mol. Syst. Biol.* **2011**, *7*, 539.
(S12) Goujon, M.; McWilliam, H.; Li, W.; Valentin, F.; Squizzato, S.; Paern, J.; Lopez, R. *Nucl. Acids Res.* **2010**, *38*, W695-W699.
(S13) Waterhouse, A. M.; Procter, J. B.; Martin, D. M.; Clamp, M.; Barton, G. J. *Bioinformatics* **2009**, *25*, 1189-1191.
(S14) The_UniProt_Consortium *Nucl. Acids Res.* **2012**, *40*, D71-75.
(S15) Chattopadhyaya, R.; Meador, W. E.; Means, A. R.; Quiocho, F. A. *J. Mol. Biol.* **1992**, *228*, 1177-1192.
(S16) Meador, W. E.; Means, A. R.; Quiocho, F. A. *Science* **1992**, *257*, 1251-1255.
(S17) Grishaev, A.; Anthis, N. J.; Clore, G. M. *J. Am. Chem. Soc.* **2012**, *134*, 14686-14689.